Seasonality Extraction by Function Fitting to Time-Series of Satellite Sensor Data

Per Jönsson and Lars Eklundh

Abstract—A new method for extracting seasonality information from time-series of satellite sensor data is presented. The method is based on nonlinear least squares fits of asymmetric Gaussian model functions to the time-series. The smooth model functions are then used for defining key seasonality parameters, such as the number of growing seasons, the beginning and end of the seasons, and the rates of growth and decline. The method is implemented in a computer program TIMESAT and tested on Advanced Very High Resolution Radiometer (AVHRR) normalized difference vegetation index (NDVI) data over Africa. Ancillary cloud data [clouds from AVHRR (CLAVR)] are used as estimates of the uncertainty levels of the data values. Being general in nature, the proposed method can be applied also to new types of satellite-derived time-series data.

Index Terms—Advanced Very High Resolution Radiometer (AVHRR), clouds from AVHRR (CLAVR), data smoothing, function fitting, normalized difference vegetation index (NDVI), phenology, satellite sensor data, seasonality, TIMESAT, time-series.

I. INTRODUCTION

IT IS RECOGNIZED that time-series of normalized difference vegetation index (NDVI) [1]–[3] data from the National Oceanic and Atmospheric Administration (NOAA) Advanced Very High Resolution Radiometer (AVHRR) spectral measurements carry useful information about the seasonal vegetation development, and that this information will aid analyses of the functional and structural characteristics of the land cover [4]–[7]. Temporal vegetation information on a global scale is important for strengthening our current knowledge concerning global cycles of matter, such as moisture and carbon dioxide [8]–[10]. Long time-series of NDVI data can also provide information concerning shifts in the spatial distribution of bioclimatic zones, indicating variations in large-scale circulation patterns or land-use changes.

Although the value of time-series data for monitoring vegetation seasons has been firmly established [5], [7], only a limited number of methods for exploring and extracting seasonality parameters from such data series have been developed. In this paper, a new and accurate method for extracting phenological parameters is presented. The method is based on nonlinear least squares fits of asymmetric Gaussian model functions directly to the time-series. The method is tested with the 8 km × 8 km pixel resolution composite ten-day Pathfinder AVHRR Land (PAL) data set generated by NASA/NOAA [11], [12]. A window covering Africa was used for the study.

II. TEMPORAL NDVI VARIATION AND SEASONALITY EXTRACTION

The main assumption behind all methods for phenological determination from satellite sensor data is that the signal is related to measures of vegetation. As such, a time-series of NDVI follows annual cycles of growth and decline. Naturally, some land surfaces, such as deserts or lakes, do not exhibit this behavior. Therefore, these surfaces are excluded from the analysis. However, it can be argued that most vegetated land surfaces, even covering evergreen areas, can be characterized by an annual cycle. A problem occurs when the quality of the NDVI signal is so low that the seasonal curve is not obvious. The PAL data in this study have been geometrically and radiometrically corrected, as well as corrected for Rayleigh scattering and ozone absorption. Nevertheless, the signal is affected by sensor disturbances, remnant geometric errors, clouds, water vapor, aerosols, surface anisotropy, and cloud shadows [13]–[17]. To reduce noise, daily data have been transformed into maximum-value composites (MVCs) (the term noise is used in a broad sense indicating disturbances in the time-series signal, and no statistical distributions are assumed). For each ten-day period, the highest NDVI is selected to represent the period [13]. The method reduces negatively biased noise due to interference of clouds and atmospheric constituents. However, residual atmospherically related noise, as well as some noise due to other factors, e.g., surface anisotropy, will remain in the data.

The most common method to extract seasonal data from NDVI time-series is based on thresholds, assuming that the growing season has started when filtered or partially smoothed NDVI values exceed a given value [18], [19]. Smoothing involves a suppression of the short-frequency variation by means of running averages, running medians, or compound smoothers [20]. A somewhat different method for suppressing noise, called the *best index slope extraction* (BISE) [21] defines an envelope by scanning a time period, ignoring low values and selecting high values, based on thresholds. In all threshold-based methods, the remaining noise may cause false starts and ends of the season, making the extracted temporal information uncertain.

P. Jönsson is with the Division of Mathematics, Natural Sciences and Language, Malmö University, Malmö, Sweden, and the Department of Physics, Lund University, Lund, Sweden (e-mail: Per.Jonsson@ts.mah.se).

L. Eklundh is with the Department of Physical Geography and Ecosystems Analysis, Lund University, Lund, Sweden (e-mail: Lars.Eklundh@nateko.lu.se).

As an alternative, seasonal data can be extracted from smooth model functions representing the data. A number of different function types and fitting methods have been used. Sellers *et al.* [22] applied Fourier smoothing by fitting the first three harmonics through the data with a least squares method. Data were empirically weighted to create an upper envelope, recognizing the fact that most noise in AVHRR NDVI time-series is negatively biased. The method was extended into a scheme named *Cloud Elimination from Composites using Albedo and NDVI Trend* (CECANT), for identifying cloud-, snow-, and smoke-covered pixels, in [23]. Along the same lines, the HANTS method was developed [24]. The usefulness of these methods depends critically on the flexibility of the model functions.

Also, classical Fourier methods have been used [25]–[31]. Based on truncated Fourier series, the number of growing seasons, the timing of seasons, and their rate of development have been extracted from AVHRR NDVI data [29], [30]. However, the irregular nature of the time-series, which is due to very high noise levels in the AVHRR NDVI data [32], [33], presents considerable difficulties.

III. METHODOLOGY

In the new method for extracting seasonality information from noisy satellite sensor data, simple local nonlinear model functions are fitted to sets of data points (t_i, I_i), $i = n_1, \ldots, n_2$, where t_i is time and I_i is NDVI. The local functions are used to build global functions that correctly describe the NDVI variation of full vegetational seasons. The method applies to data sets sampled at different rates. Therefore, for example, one can use daily data just as well as ten-day or monthly MVCs. Also, there are no restrictions on the scaling of the NDVI. In this work, ten-day composites are used, and in the figures time is always in ten-day steps measured from the beginning of the year. NDVI is expressed in scaled units according to the PAL standard, where $\mathrm{NDVI} = (\mathrm{DN} - 128) \times 0.008$.

A. Local Model Function

The adopted local model functions have the general form

$$f(t) \equiv f(t; c_1, c_2, a_1, \ldots, a_5) = c_1 + c_2 g(t; a_1, \ldots, a_5) \quad (1)$$

where

$$g(t; a_1, \ldots, a_5) = \begin{cases} \exp\left[-\left(\frac{t-a_1}{a_2}\right)^{a_3}\right], & \text{if } t > a_1 \\ \exp\left[-\left(\frac{a_1-t}{a_4}\right)^{a_5}\right], & \text{if } t < a_1 \end{cases} \quad (2)$$

is a Gaussian-type function. The linear parameters c_1 and c_2 determine the base level and the amplitude. For the Gaussian function, a_1 determines the position of the maximum or minimum with respect to the independent time variable t, while a_2 and a_3 determine the width and flatness (kurtosis) of the right function half. Similarly, a_4 and a_5 determine the width and flatness of the left half. The effects of varying the parameters $a_2, \ldots, a_5$ are shown in Fig. 1. In order to ensure smooth shapes of the model functions, consistent with what is observed for NDVI data, the parameters $a_2, \ldots, a_5$ are restricted in range. For example, a_3
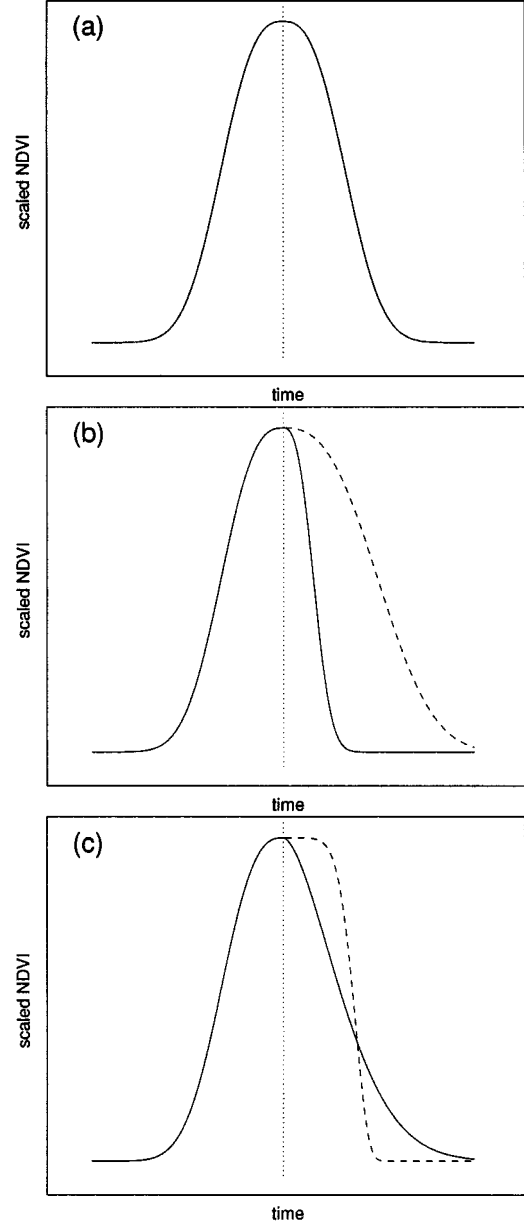

Fig. 1. Effect of parameter changes on the local functions. (a) Symmetric Gaussian function. (b) Parameter a_2, which determines the width of the right function half, has been decreased (solid line) and increased (dashed line) compared to the value in (a). (c) Parameter a_3, which determines the flatness of the right function half, has been decreased (solid line) and increased (dashed line) compared to the value in (a).

and a_5 are assumed to be larger than 2 in order to avoid a cusp at the matching point $t = a_1$ of the Gaussian function.

B. Determination of the Parameters

The local model functions are well suited for describing the shape of the scaled NDVI time-series in overlapping intervals around maxima and minima. If we select a set of data points (t_i, I_i), $i = n_1, \ldots, n_2$ in an interval around a maximum or a minimum, the parameters c_1, c_2, and $a_1, \ldots, a_5$ are obtained by minimizing the merit function

$$\chi^2 = \sum_{i=n_1}^{n_2} \left[\frac{f(t_i; c_1, c_2, a_1, \ldots, a_5) - I_i}{\sigma_i} \right]^2 \quad (3)$$

where σ_i is the measurement uncertainty of the ith data point, presumed to be known. If the measurement uncertainties are not known, they may all be set to the constant value $\sigma = 1$. To estimate the uncertainty of the NDVI data points, the PAL cloud flag channel CLAVR was used in this study. CLAVR is formed by an algorithm that uses reflected and thermal AVHRR wavelength bands to classify pixels into clear, mixed, and cloudy categories [34], [35].

C. Adopting to the Upper Envelope

To take into account the fact that most noise, even for data classified as clear by CLAVR, is negatively biased, the determination of the parameters of the model function is done in two steps. In the first step, the parameters are obtained by minimizing the merit function with σ_i as obtained from the ancillary data. Data points below the model function of the first fit are thought of as being less important, and in the second step the minimization is redone with the σ_i of the low data points increased by a factor of two. This two-step procedure leads to a model function that is adopted to the upper envelope of the NDVI data (see Fig. 2).

D. Global Model Function

The local model functions describe NDVI data very well in broad intervals around maxima and minima. At the limbs, however, the fits are less good. If we denote the local functions describing the NDVI variation in intervals around the left minima, the central maxima, and the right minima by $f_L(t)$, $f_C(t)$, and $f_R(t)$ [see Fig. 3(a)–(c)], the global function $F(t)$ that correctly models the NDVI variation in full interval $[t_L, t_R]$ is

$$F(t) = \begin{cases} \alpha(t)f_L(t) + [1 - \alpha(t)]f_C(t), & t_L < t < t_C \\ \beta(t)f_C(t) + [1 - \beta(t)]f_R(t), & t_C < t < t_R \end{cases}.$$

Here, $\alpha(t)$ and $\beta(t)$ are cutoff functions that in small intervals around $(t_L + t_C)/2$ and $(t_C + t_R)/2$, respectively, smoothly drop from 1 to 0. Loosely speaking, the global function $F(t)$, shown in Fig. 3(d), assumes the character of $f_L(t)$, $f_C(t)$, and $f_R(t)$ in, respectively, the left, central, and right part of the interval $[t_L, t_R]$. The merging of local functions to a global function is a key feature of the method. It increases the flexibility and allows the fitted function to follow a complex behavior of the time-series. An example of this is given in Fig. 4, where data are characterized by a distinct peak followed by a plateau. This behavior cannot be represented by a single Gaussian or by a low-order Fourier method.

IV. IMPLEMENTATION OF THE METHOD

The method is implemented by the user in a general computer program TIMESAT that processes NDVI data for pixels in a selected geographical area. Below are some comments on the different parts of the program.

A. Determination of σ_i

The data points of the CLAVR time-series are categorized as clear, mixed, and cloudy. The measurement uncertainties σ_i of the corresponding NDVI values are then set to 1, 2, and 100, respectively. These values are provisional and can be changed.
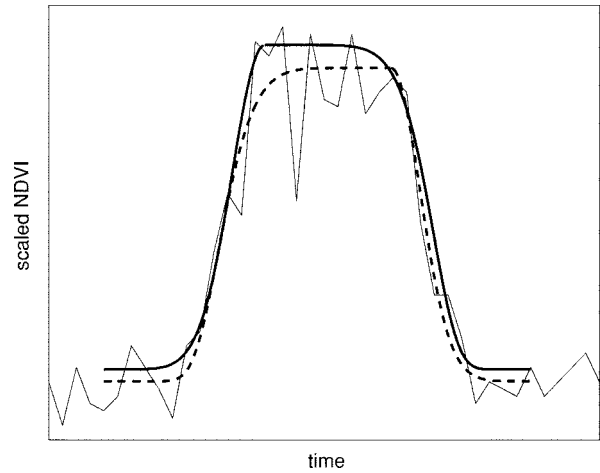

Fig. 2.   Fitted functions around a maximum from the two-step procedure. The dashed line shows the fitted function from the first step, and the solid line the fit from the second step. The original NDVI time-series is shown by the noisy fine continuous line.

B. Running Window Averaging

Several of the algorithms in TIMESAT, especially the ones used to find a consistent set of maxima and minima, rely on smoothed NDVI values $\tilde{I}_i$, $i = n_1, \ldots, n_2$. Currently, the smoothing is done using a running window-averaging procedure

$$\tilde{I}_i = \frac{\left[\sum_{n=-n_L}^{n_R} c_n I_{i+n} \right]}{\sum_{n=-n_L}^{n_R} c_n} \tag{4}$$

where n_L and n_R are the number of points used to the left and right of the data point i. For the data set used in this study, the window parameters n_L and n_R were set to three. Taking the ancillary CLAVR data into account, the weights of the averaging are set to $c_n = 1/\sigma_n$.

C. Performing Quality Checks on Time-Series

In order to process the time-series, some basic quality criteria must be fulfilled. First, checks are done on missing data. Time-series with too many missing data points, or where the number of contiguous missing values exceeds a threshold value, are discarded. Second, extreme spikes of single high or low values (usually related to sensor disturbances) are removed. Third, tests are performed to detect a low overall signal variation, which is typical for desert areas. Time-series for which the difference between the maximum and minimum values of the smoothed NDVI divided by the mean value falls below a threshold value are discarded. Fourth, the program looks for time-series with a high degree of noise. Currently, time-series are removed when the ratio of the sum of squared distances between the original and smoothed NDVI data values to the mean value exceed a selected threshold. Such noise may be found in some humid tropical areas.

The four checks are done to ensure that only pixels with a clearly recognizable seasonal curve are passed on to the
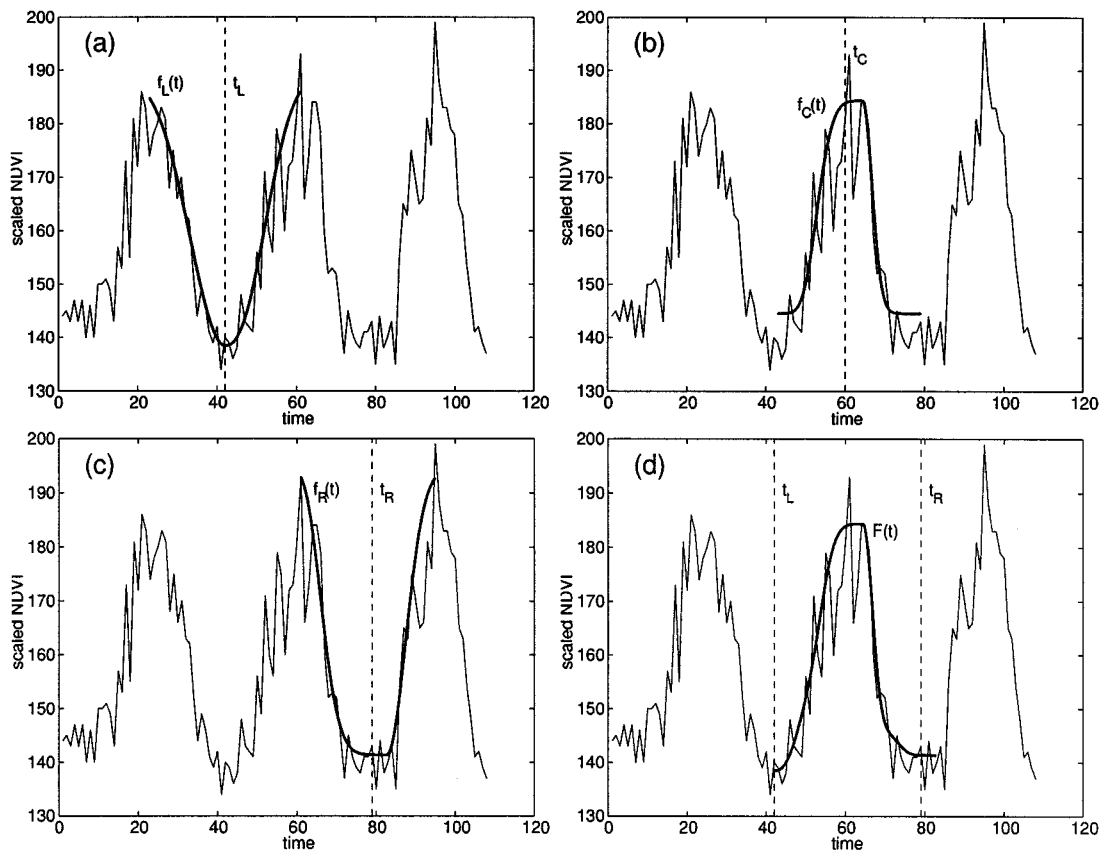
Fig. 3. Scaled NDVI covering a time period of three years for a selected location in Africa. Time is expressed in ten-day steps. Year 1 goes between 1 and 36, year 2 between 36 and 72, and year 3 between 72 and 108. (a)–(c) Local model functions fitted to the left minimum, the central maximum, and the right minimum. (d) Global model function $F(t)$ that is obtained by merging the three local functions. The global function assumes the character of the three local functions $f_L(t)$, $f_C(t)$, and $f_R(t)$ in, respectively, the left, central, and right part of the interval $[t_L, t_R]$.
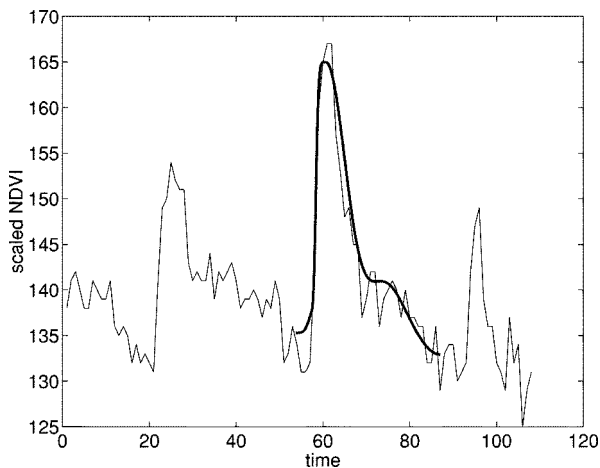

Fig. 4. Global function fitted to a time-series with a distinct peak followed by a decaying plateau.

curve-fitting subroutines. The criteria can be relaxed, and the extreme is to process all data, except for the very small fraction, less than one pixel out of a thousand, for which the nonlinear fit fails. The relaxation might force the program to fit functions to time-series where no actual seasonal curve is present and where the obtained result is of limited interest.

D. Selecting Consistent Sets of Maxima and Minima

Based on smoothed data from the running window-averaging procedure, a consistent set of maxima and minima, to which the local functions are fitted, is identified. Checks done ensure that the differences in time and intensity between maxima and minima are reasonable. Of course, finding maxima and minima becomes more subjective for noisy data or for data from areas where there is no clear seasonality.

E. Fitting Local Model Functions

To ensure that the limbs of the seasons are correctly modeled, three years of data are used. The functions are fitted to the seasons of the central year, but the seasons may spill over to the adjacent years.

The parameters of the local model functions are determined by minimizing the merit function χ^2. To find the minimum of the merit function, a grid search [36] is done over the region of allowed values of the nonlinear parameters $a_1, \ldots, a_5$. For each combination of the nonlinear parameters, the linear parameters c_1 and c_2 are obtained by solving the normal equations of the linear least squares problem [36]. The parameter combination giving the smallest value of the merit function is then used as the starting value for the full Newton-type minimization code NL2SOL [37], [38], which is used to provide the final solution.
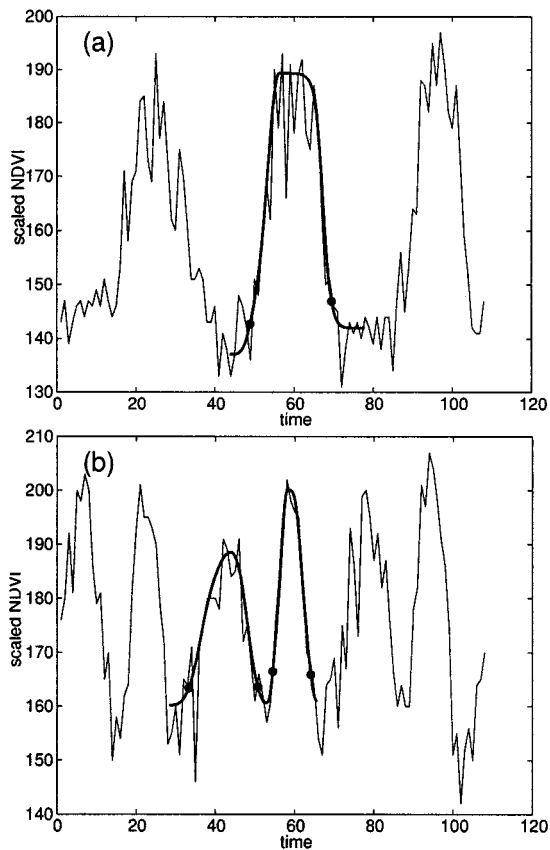
Fig. 5. Global functions fitted to NDVI data with (a) one and (b) two annual growing seasons. The beginnings and ends of the seasons are marked by circles.

F. Extracting Phenological Data

Phenological data are extracted for each of the growing seasons of the central year. The beginning of a season is defined from the global model function as the point in time for which the value has increased by a certain value, currently set to 10% of the distance between the base level and the maximum, above the base level. The end of the season is defined in a similar way.

The rate of increase in NDVI during the beginning of the season is theoretically related to the physiognomy of the vegetation and can be estimated by the first derivative between the minimum and the maximum NDVI values. The rate of decrease after the maximum NDVI also holds phenologically relevant information and can be estimated in a similar way. In TIMESAT, the derivatives are determined at points midway between the base level and the maximum value.

The annual integrated NDVI is frequently used as a measure of net primary production [8], [39], [40]. To give a good estimate of the production of the phenologically dominant vegetation type, the time of integration is restricted to the growing seasons.

Among the other phenological parameters extracted are the amplitude of the signal, the maximum signal value and its date, and the length of the growing season.

V. RESULTS

TIMESAT was tested on ten-day MVC AVHRR NDVI data for Africa for the time period 1982 to 2000. Fig. 5 shows time-
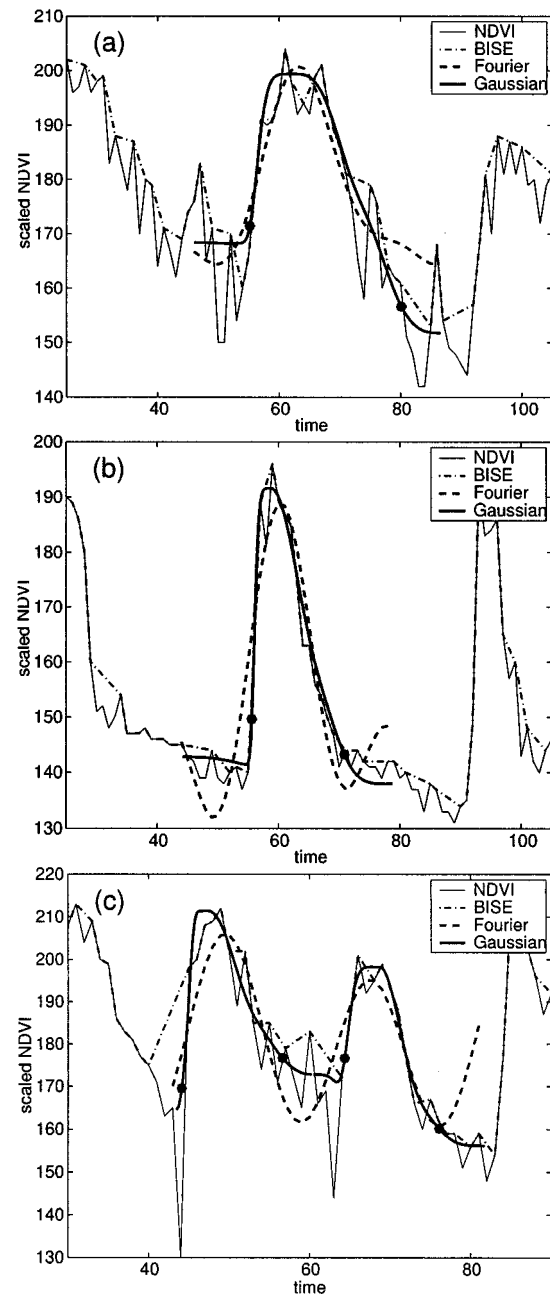

Fig. 6. Comparisons with other methods. Global model functions are displayed along with curves from BISE with a sliding window of four ten-day periods and with functions obtained from upper envelope weighted least squares fits to three Fourier components. The beginnings and ends of the seasons, as obtained by the Gaussian functions, are marked by circles. The plots are zoomed in on the central year. In (a), the small peak around decade 45 may give a false season start for BISE combined with threshold criteria. In (b), the narrow peak gives rise to spurious oscillations for the Fourier method. In (c), BISE fails to give an accurate value of the season start.

series with, respectively, one and two annual growing seasons for which the program successfully fitted global functions. From the model functions, the beginning and end of the seasons were extracted. It can be seen that the two fitted global functions of the time-series in Fig. 5(b) are dissimilar, and that the left function is clearly asymmetric. These properties can be useful as an aid in the determination of the functional type of vegetation. Clearly, an asymmetric signal can also be an indicator of fire or human management, including agricultural practices
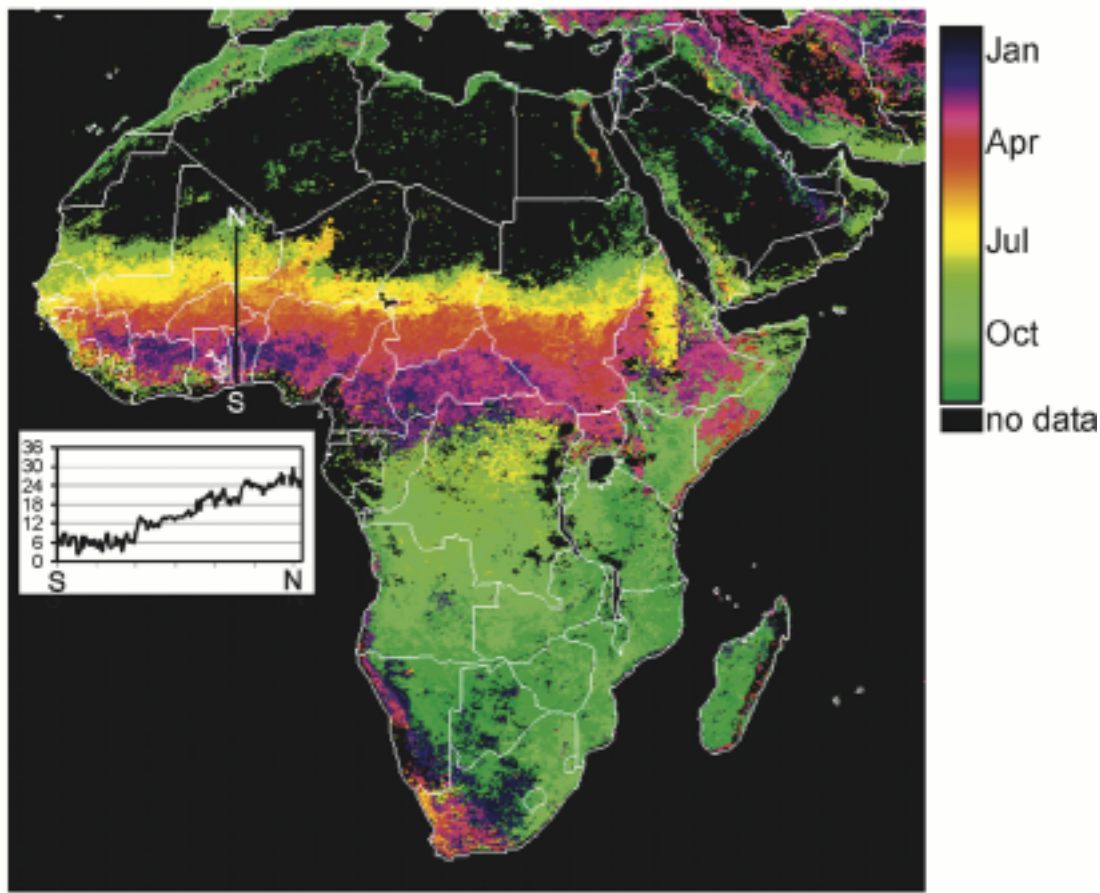
Fig. 7.   Start of the first growing season of 1991, estimated from the fitted functions. Time is in decades going from 1 (January 1–10) to 36 (December 21–31). The small graph shows the variation in date over the marked transect across the Sahel.

such as harvest. In Fig. 6(a)–(c), fitted global functions are displayed together with functions from an upper envelope weighted least squares fit to three Fourier components and with smoothed curves using BISE. From the figure, it is clear that the asymmetric Gaussian functions are more flexible than are the sinus and cosinus basis of the Fourier methods, and that the global model function of the present method does very well in determining the start and end of the seasons in all three cases. It should also be noted the global model function built from Gaussians is able to follow the narrow peak of the time-series in Fig. 6(b) without the spurious oscillations that are connected with Fourier series. Turning to BISE, it is seen that this method combined with some threshold criteria is doing very well in determining the start and end of the time-series in Fig. 6(b). The remaining noise in Fig. 6(a) and (c), however, presents major difficulties. In these time-series, determination of the start, maximum, and end of the seasons would be inaccurate with BISE.

The real usefulness of the new method depends on the ability to generate spatially coherent images of phenological parameters. Two examples of this ability are given in Figs. 7 and 8. Fig. 7 was generated from beginnings of the first growing season of 1991. The colors represent the ten-day period of the start, and they vary from 1 (January 1–10) to 36 (December 21–31). Black pixels represent missing data or areas where no clear seasonal signal was found. A profile has been drawn from the South Atlantic through the Sahel to the Sahara. The line chart in Fig. 7

gives the pixel values for this profile. Near the coast the season starts around decade 5 (end of February). The starting date then shifts toward later dates until the border of the Sahara, where it falls at about decade 25 (beginning of October). The overall patterns in Fig. 7 appear to be in general agreement with the climatic patterns, which in Africa are dominated by the movements of the intertropical convergence zone (ITCZ) [41].

Fig. 8 displays the amplitude of the first growing season of 1991. The lowest amplitudes are found in and around desert areas, where the overall values of NDVI are very low. The highest amplitudes are found in semi-arid areas, where the vegetation development follows a marked annual cycle of growth and decline coupled to the rainfall variations. In moist areas, e.g., parts of West Africa and areas close to the equator, the amplitude is fairly low. In these areas, rainfall is more abundant and more evenly distributed over the year, resulting in a weaker seasonal variation in vegetation greenness.

VI. SUMMARY AND DISCUSSION

A method to fit asymmetric Gaussian functions to time-series of satellite sensor data is presented. The fitted functions are used to portray the seasonal growth and decline curves of the land vegetation, and to estimate phenological parameters. With a method to map phenological variables over very large areas,
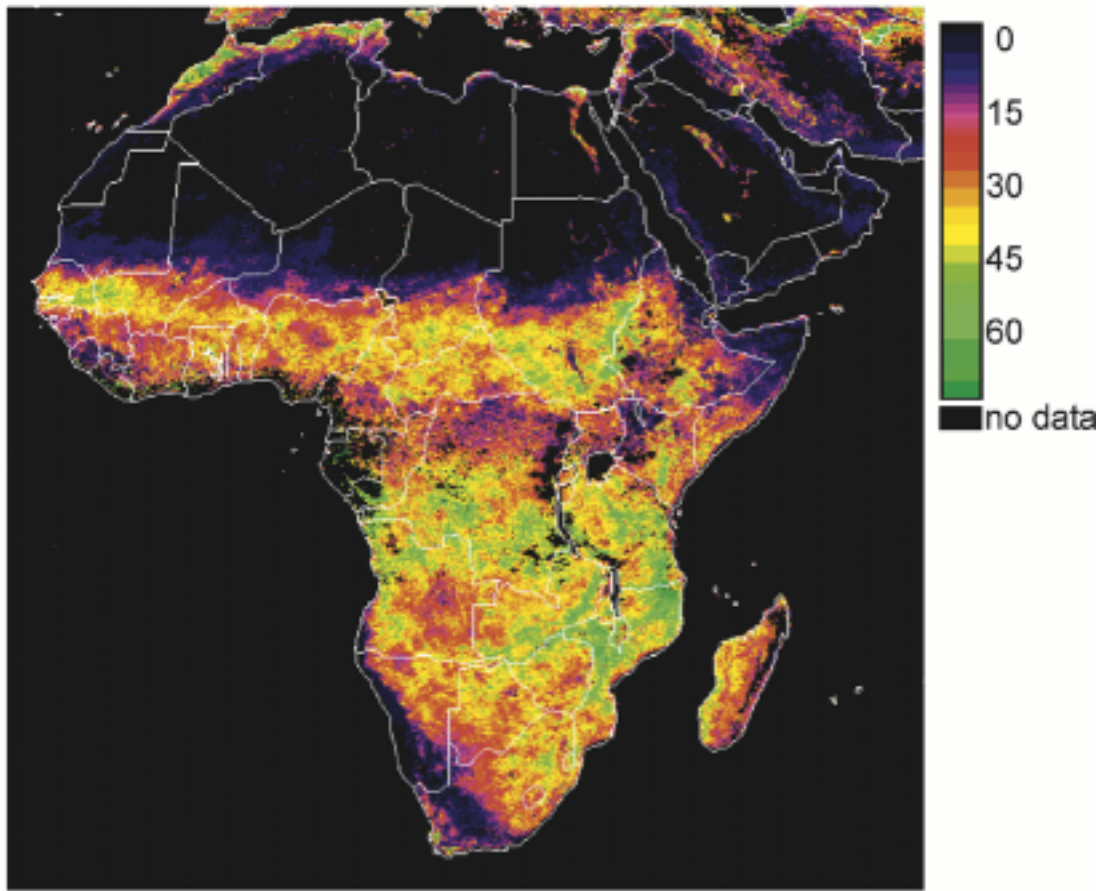
Fig. 8.   Amplitude of the scaled NDVI values of the first growing season of 1991. The amplitude was computed as the difference between the maximum value of the fitted function and the average of the left- and right-hand side minimum values.

the possibilities of correctly determining land cover and vegetation types, and estimating biophysical parameters on regional and global levels, increase. This will aid the provision of useful remotely sensed input data to global and regional biogeochemical models.

The function fitting is improved by bringing in ancillary data in the form of CLAVR fields. These data provide a qualitative indicator of the cloud status of each data point in the time-series, and they can be translated to an uncertainty estimate σ_i of the NDVI value. CLAVR is a provisional data set that has been shown to underestimate the number of clear pixels [42]. Other cloud classifications, such as CLAVR-3 [42], or regionally adapted schemes could also be used. The new method was developed to extract phenological parameters, but it can also be used to reconstruct a smooth time-series. To this end, it compares favorably with BISE and methods based on Fourier series.

A difficulty in the method, as implemented in the program TIMESAT, is to make an unambiguous identification of the true maxima and minima in the time-series, i.e., to discriminate between the maxima and minima that come from the underlying seasonal variation and the maxima and minima that may result from noise or disturbances. This is currently solved by making a search of the moving average filtered data. In [25], the maxima and minima were identified from the first three Fourier components. The method was generally successful, except where

the noise level was high or where the growing season was very short. In light of these results, one possible way to improve the method for identifying true maxima and minima would be to fit Fourier series to several years of NDVI data, determining the average number of seasons. This information could then aid the algorithms of TIMESAT. Work is currently underway along these lines.

NDVI was used in this study, but other vegetation indices that follow the seasonal variation of land vegetation can also be processed. Currently, the only data assumption is that most of the noise in the data has a negative bias. If this assumption is not met, the weighting procedure in the iteration step should be altered.

It can be argued that it is necessary to make a full correction for atmospheric and BRDF effects before extracting phenological information. If ancillary data for correcting for these effects exist, the improved signal quality will generate more correct phenological parameters and improve the Gaussian function fits. When processing long time-series, trends due to solar zenith angle variations, atmospheric aerosols from volcanic eruptions, or other slowly varying systematic errors will affect seasonal integrals and maximum values that are additive quantities. Other metrics, such as the dates of the seasons, however, will remain stable.

New long-term databases with improved spatial and spectral characteristics will be constructed as data from new and planned

systems, such as Terra MODIS, SPOT Vegetation, and Envisat MERIS, are compiled. TIMESAT was developed to work with such data sets without major alterations.

Although outside the scope of this paper, a necessary research topic will be to validate the seasonality metrics and to estimate their significance by comparing with vegetation and climate data. Validation is, however, very difficult to carry out due to the large pixel size of the data. It also remains to be tested if the form of the model functions is well adapted to describe time-series of other biomes than the currently tested ones, e.g., Northern Boreal forests.

ACKNOWLEDGMENT

REFERENCES

[1] J. W. J. Rouse, R. H. Haas, J. A. Schell, and D. W. Deering, "Monitoring vegetation systems in the Great Plains with ERTS," in *Proc. 3rd ERTS Symp., NASA SP-351*, Washington, DC, Dec. 10–14, 1974, pp. 309–317.

[2] C. J. Tucker, "Red and photographic infrared linear combinations for monitoring vegetation," *Remote Sens. Environ.*, vol. 8, pp. 127–150, 1979.

[3] B. N. Holben, C. J. Tucker, and C. J. Fan, "Spectral assessment of soybean leaf area and leaf biomass," *Photogramm. Eng. Remote Sens.*, vol. 46, pp. 651–656, 1980.

[4] C. O. Justice, J. R. G. Townshend, B. N. Holben, and C. J. Tucker, "Analysis of the phenology of global vegetation using meteorological satellite data," *Int. J. Remote Sens.*, vol. 6, pp. 1271–1318, 1985.

[5] J.-P. Malingreau, "Global vegetation dynamics: Satellite observations over Asia," *Int. J. Remote Sens.*, vol. 7, pp. 1121–1146, 1986.

[6] J. R. G. Townshend and C. O. Justice, "Analysis of the dynamics of African vegetation using the normalized difference vegetation index," *Int. J. Remote Sens.*, vol. 7, pp. 1435–1445, 1986.

[7] C. J. Tucker, C. O. Justice, and S. D. Prince, "Monitoring the grasslands of the Sahel 1984–1985," *Int. J. Remote Sens.*, vol. 7, pp. 1571–1581, 1986.

[8] S. W. Running and R. R. Nemani, "Relating seasonal patterns of the AVHRR vegetation index to simulated photosynthesis and transpiration of forests in different climates," *Remote Sens. Environ.*, vol. 24, pp. 347–367, 1988.

[9] Å. Rosenqvist, M. Imhoff, A. Milne, and C. Dobson, "Remote sensing and the kyoto protocol—A workshop summary," in *International Archives of Photogrammetry and Remote Sensing*, vol. XXXIII, Amsterdam, The Netherlands, 2000, pp. 1278–1285.

[10] P. J. Sellers, R. E. Dickinson, D. A. Randall, A. K. Betts, F. G. Hall, J. A. Berry, G. J. Collatz, A. S. Denning, H. A. Mooney, C. A. Nobre, N. Sato, C. B. Field, and A. Henderson-Sellers, "Modeling the exchanges of energy, water, and carbon between continents and the atmosphere," *Science*, vol. 275, pp. 502–509, 1997.

[11] J. R. G. Townshend, "Global data sets for land applications from the advanced very high resolution radiometer: An introduction," *Int. J. Remote Sens.*, vol. 15, pp. 3319–3332, 1994.

[12] M. E. James and S. N. V. Kalluri, "The Pathfinder AVHRR Land data set: An improved coarse resolution data set for terrestrial monitoring," *Int. J. Remote Sens.*, vol. 15, pp. 3347–3363, 1994.

[13] B. N. Holben, "Characteristics of maximum-value composite images from temporal AVHRR data," *Int. J. Remote Sens.*, vol. 7, pp. 1417–1443, 1986.

[14] S. D. Prince and S. N. Goward, "Evaluation of the NOAA/NASA Pathfinder AVHRR Land data set for global primary production modeling," *Int. J. Remote Sens.*, vol. 17, pp. 217–221, 1996.

[15] G. G. Gutman, "Vegetation indices from AVHRR: An update and future prospects," *Remote Sens. Environ.*, vol. 35, pp. 121–136, 1991.

[16] D. Tanré, B. N. Holben, and Y. J. Kaufman, "Atmospheric correction algorithm for NOAA AVHRR products: Theory and application," *IEEE Trans. Geosci. Remote Sensing*, vol. 30, pp. 231–248, Mar. 1992.

[17] J. J. Simpson and J. R. Stitt, "A procedure for the detection and removal of cloud shadow from AVHRR data over land," *IEEE Trans. Geosci. Remote Sensing*, vol. 36, pp. 880–897, May 1998.

[18] D. Lloyd, "A phenological classification of terrestrial vegetation cover using shortwave vegetation index imagery," *Int. J. Remote Sens.*, vol. 11, pp. 2269–2279, 1990.

[19] B. C. Reed, J. F. Brown, D. VanderZee, T. R. Loveland, J. W. Merchant, and D. O. Ohlen, "Measuring phenological variability from satellite imagery," *J. Veg. Sci.*, vol. 5, pp. 703–714, 1994.

[20] A. van Dijk, S. L. Callis, C. M. Sakamoto, and W. L. Decker, "Smoothing vegetation index profiles: An alternative method for reducing radiometric disturbance in NOAA/AVHRR data," *Photogramm. Eng. Remote Sens.*, vol. 53, pp. 1059–1067, 1987.

[21] N. Viovy, O. Arino, and A. S. Belward, "The best index slope extraction (BISE): A method for reducing noise in NDVI time-series," *Int. J. Remote Sens.*, vol. 13, pp. 1585–1590, 1992.

[22] P. J. Sellers, C. J. Tucker, G. J. Collatz, S. O. Los, C. O. Justice, D. A. Dazlich, and D. A. Randall, "A global $1° \times 1°$ NDVI data set for climate studies—Part II: The generation of global fields of terrestrial biophysical parameters from the NDVI," *Int. J. Remote Sens.*, vol. 15, pp. 3519–3545, 1994.

[23] J. Cihlar, "Identification of contaminated pixels in AVHRR composite images for studies of land biosphere," *Remote Sens. Environ.*, vol. 56, pp. 149–153, 1996.

[24] G. J. Roerink, M. Menenti, and W. Verhoef, "Reconstructing cloudfree NDVI composites using Fourier analysis of time series," *Int. J. Remote Sens.*, vol. 21, pp. 1911–1917, 2000.

[25] L. Olsson and L. Eklundh, "Fourier series for analysis of temporal sequences of satellite sensor imagery," *Int. J. Remote Sens.*, vol. 15, pp. 3735–3741, 1994.

[26] M. Menenti, S. Azzali, W. Verhoef, and R. van Swol, "Mapping agroecological zones and time lag in vegetation growth by means of Fourier analysis of time series of NDVI images," *Adv. Space Res.*, vol. 13, pp. 233–237, 1993.

[27] ———, "Mapping agroecological zones and time lag in vegetation growth by means of Fourier analysis of time-series of NDVI images," DLO, The Winand Staring Centre, Wageningen, Sweden, Rep. 32, 1991.

[28] L. Andres, W. Salas, and D. Skole, "Fourier analysis of multi-temporal AVHRR data applied to a land cover classification," *Int. J. Remote Sens.*, vol. 15, pp. 1115–1121, 1994.

[29] L. Eklundh, "Analyzing phenological behavior of vegetation with AVHRR NDVI imagery using Fourier series," in *Proc. Meteorological Satellite Data Users' Conf.*, Winchester, U.K., Sept. 4–8, 1995, pp. 163–170.

[30] ———, "Analyzing global vegetation seasons using high time-resolution satellite sensor data," in *Proc. 27th Int. Symp. Remote Sensing of Environment*, 1998, pp. 262–265.

[31] A. Moody and D. Johnson, "Land-surface phenologies from AVHRR using the discrete Fourier transform," *Remote Sens. Environ.*, pp. 305–323, 2001.

[32] L. Eklundh, "Noise estimation in NOAA AVHRR maximum-value composite NDVI images," *Int. J. Remote Sens.*, vol. 16, pp. 2955–2962, 1995.

[33] A. Chappell, J. W. Seaquist, and L. Eklundh, "Improving the estimation of noise from NOAA AVHRR NDVI for Africa using geostatistics," *Int. J. Remote Sens.*, vol. 22, pp. 1067–1080, 2001.

[34] L. L. Stowe, E. P. McClain, R. Carey, P. Pellegrino, G. Gutman, P. Davis, C. Long, and S. Hart, "Global distribution of cloud cover derived from NOAA/AVHRR operational satellite data," *Adv. Space Res.*, vol. 3, pp. 51–54, 1991.

[35] G. Gutman and A. Ignatov, "The relative merit of cloud/clear identification in the NOAA/NASA Pathfinder AVHRR Land 10-day composites," *Int. J. Remote Sens.*, vol. 17, pp. 3295–3304, 1996.

[36] J. O. Rawlings, S. G. Pantula, and D. A. Dickey, *Applied Regression Analysis*. New York: Springer-Verlag, 1998.

[37] J. E. Dennis, D. M. Gay, and R. E. Welsch, "An adaptive nonlinear least-squares algorithm," *ACM Trans. Math. Softw.*, vol. 7, pp. 348–368, 1981.

[38] ———, "Algorithm 573, NL2SOL—An adaptive nonlinear least-squares algorithm [E4]," *ACM Trans. Math. Softw.*, vol. 7, pp. 369–383, 1981.

[39] S. N. Goward and D. G. Dye, "Evaluating North American net primary productivity with satellite observations," *Adv. Space Res.*, vol. 7, pp. 165–174, 1987.

[40] A. Ruimy, B. Saugier, and G. Dedieu, "Methodology for the estimation of terrestrial net primary production from remotely sensed data," *J. Geophys. Res.*, vol. 99, pp. 5263–5283, 1994.

[41] H. E. Landsberg, Ed., *Climates of Africa. World Survey of Climatology*. Amsterdam, The Netherlands: Elsevier, 1972, vol. 10.

[42] S. Vemury, L. Stowe, and V. Anne, "AVHRR pixel level clear-sky classification using dynamic thresholds (CLAVR-3)," *J. Atmos. Ocean. Technol.*, vol. 18, pp. 169–186, 2001.

IEEE TRANSACTIONS ON GEOSCIENCE AND REMOTE SENSING, VOL. 40, NO. 8, AUGUST 2002

Per Jönsson received the Ph.D. degree in physics from Lund University, Lund, Sweden, in 1995.

He is currently Associate Professor with the Department of Physics, Lund University, and Lecturer in Applied Mathematics at Malmö University, Malmö, Sweden. From 1995 to 1997, he was a Postdoctoral Research Assistant in computer science at Vanderbilt University, Nashville, TN. His research interests are in theoretical atomic physics and astrophysics.

Lars Eklundh received the B.S. degree in earth science/physical geography and the Ph.D. degree physical geography, both from Lund University, Lund, Sweden, in 1985 and 1996, respectively.

He is currently a Research Associate at Lund University. He was with the United Nations Environment Programme (UNEP) from 1989 to 1992. His primary research interest is remote sensing for extraction of information from land surfaces and the analysis of spatial and temporal variation of vegetation parameters. He is currently funded by the Swedish National Space Board for a research program on the extraction of vegetation parameters from remotely sensed data for carbon balance modeling.